The cryo-EM structure of African swine fever virus unravels a unique architecture comprising two icosahedral protein capsids and two lipoprotein membranes

German Andrés[‡1,2], Diego Charro[§1], Tania Matamoros[‡], Rebecca S. Dillard[¶], and Nicola G. A. Abrescia[§‖3]

From the ‡Centro de Biología Molecular Severo Ochoa, CSIC and Universidad Autónoma de Madrid, 28049 Madrid, Spain, the §Molecular Recognition and Host–Pathogen Interactions Programme, CIC bioGUNE, CIBERehd, Bizkaia Technology Park, 48160 Derio, Spain, ¶NeCEN, Institute of Biology Leiden, Leiden University, 2333 CC Leiden, Netherlands, and ‖IKERBASQUE, Basque Foundation for Science, 48013 Bilbao, Spain

Edited by Craig E. Cameron

African swine fever virus (ASFV) is a complex nucleocytoplasmic large DNA virus (NCLDV) that causes a devastating swine disease currently present in many countries of Africa, Europe, and Asia. Despite intense research efforts, relevant gaps in the architecture of the infectious virus particle remain. Here, we used single-particle cryo-EM to analyze the three-dimensional structure of the mature ASFV particle. Our results show that the ASFV virion, with a radial diameter of ∼2,080 Å, encloses a genome-containing nucleoid surrounded by two distinct icosahedral protein capsids and two lipoprotein membranes. The outer capsid forms a hexagonal lattice (triangulation number T = 277) composed of 8,280 copies of the double jelly-roll major capsid protein (MCP) p72, arranged in trimers displaying a pseudo-hexameric morphology, and of 60 copies of a penton protein at the vertices. The inner protein layer, organized as a T = 19 capsid, confines the core shell, and it is composed of the mature products derived from the ASFV polyproteins pp220 and pp62. Also, an icosahedral membrane lies between the two protein layers, whereas a pleomorphic envelope wraps the outer capsid. This high-level organization confers to ASFV a unique architecture among the NCLDVs that likely reflects the complexity of its infection process and may help explain current challenges in controlling it.

African swine fever virus (ASFV)[4] is the causative agent of a highly lethal hemorrhagic disease of domestic pigs, for which there is no vaccine or antiviral strategy available. The disease is currently present in many countries of sub-Saharan Africa, Eastern Europe, and East Asia, threatening the pig industry and food security worldwide (1, 2) (http://www.fao.org/ag/againfo/programmes/en/empres/ASF/index.html).[5]

ASFV is the sole member of the *Asfarviridae* family of the proposed order "*Megavirales*," a monophyletic, albeit heterogeneous, clade of nucleocytoplasmic large DNA viruses (NCLDVs) that form the most complex group of DNA viruses known so far (4, 5). At present, the NCLDV group contains eight taxonomic families (*Ascoviridae, Asfarviridae, Iridoviridae, Marseilleviridae, Mimiviridae, Phycodnaviridae, Pithoviridae, and Poxviridae*), a number that will probably increase in the near future due to the continuous discovery of new, not yet classified, giant viruses like pandoraviruses (6), faustoviruses (7), mollivirus (8), kaumoebavirus (9), cedratviruses (10), and pacmanvirus (11).

NCLDVs display a broad host tropism that includes phagotrophic protists like amoebas, plants like green algae, and animals like insects, reptiles, and mammals. ASFV mainly infects wild and domestic pigs, as well as tick vectors of the genus *Ornithodoros*, being the only known DNA arbovirus. The viral genome is a dsDNA molecule of 170–190 kbp that contains 151–167 ORFs, depending on the virus strain (12, 13). The ASFV particle contains about 70 different polypeptides, including multiple structural components, as well as a full set of enzymes and factors involved in viral transcription (14). Earlier structural studies based on aldehyde-fixed samples anticipated that the virion consists of an external lipid membrane, an icosahedral protein capsid, an internal lipid membrane, a thick protein core shell, and a genome-containing nucleoid (15–17).

ASFV infects porcine monocytes and macrophages and replicates in specialized cytoplasmic areas close to the nucleus,

SASBMB

J. Biol. Chem. (2020) 295(1) 1–12 **1**

known as viral factories (16). In these assembly sites, intracellular particles acquire their inner membrane from endoplasmic reticulum membrane fragments (18, 19). Viral membranes become icosahedral particles by the progressive building of the outer capsid, which is essentially composed by the major capsid protein (MCP) p72 and the minor protein p49 (20, 21). Concomitantly, the core shell, which is made of the mature products derived from polyproteins pp220 and pp62, and the genome-containing nucleoid are enclosed (16, 22, 23). Once formed, intracellular icosahedral mature particles move to the cell surface by a microtubule-mediated transport system and exit the cell by budding at the plasma membrane while acquiring their outer envelope (Fig. 1A). Both intracellular and extracellular ASFV forms are infectious, which indicates that the external membrane is not strictly necessary for infectivity (24).

Many of the NCLDVs, including the phycodnavirus *Paramecium bursaria* Chlorella virus (PBCV-1) (25), the iridovirus *Chilo* iridescent virus (CIV) (26), the mimivirus *Cafeteria roenbergensis* virus (CroV) (27), or the giant amoeba-infecting Faustovirus (28), Pacmanvirus (11), and Medusavirus (29), present large icosahedral capsids composed of trimers of a MCP that displays a double jelly-roll fold. Each jelly-roll structure consists of eight anti-parallel β-strands arranged in two four-stranded sheets (30); the trimeric capsomer thus displays a pseudo-hexameric morphology. Similar capsid structures are found in other dsDNA viruses such as adenoviruses and the tailless membrane-containing bacteriophage PRD1 (31, 32).

Other NCLDVs with non-icosahedral architectures include the amphora-shaped pandoraviruses and pithoviruses, the spherical molliviruses (33), and the brick-shaped poxviruses, which, interestingly, use a double jelly-roll scaffolding protein, D13, during their assembly (34).

Most of the NCLDVs, including ASFV and its distant relative Pacmanvirus (11), have an internal membrane surrounding the genome-containing core. A prominent exception is represented by ASFV's closest relative, Faustovirus, which lacks a lipid membrane but contains two concentric icosahedral capsids (28).

Here, we have used single-particle cryo-EM to characterize the three-dimensional (3D) structure of the extracellular mature ASFV particle and of the virion-derived homotrimeric p72 capsomers. Our cryo-EM study shows that the ASFV virion contains two distinct icosahedral proteinaceous capsids and two lipoprotein membranes. The outer capsid resolved at $\sim$23 Å resolution, which is wrapped by a pleomorphic external envelope, is organized in trisymmetrons and pentasymmetrons with pseudo-hexameric capsomers composed of homotrimers of double jelly-roll p72 protein (visualized at $\sim$5 Å resolution) arranged on a hexagonal lattice with a triangulation number $T = 277$. Juxtaposed to the base of the outer capsid, there is an icosahedrally ordered membrane that encloses an inner capsid whose pseudo-hexameric capsomers arrange on a $T = 19$ hexagonal lattice. This internal capsid, which is made of some mature products derived from ASFV polyproteins pp220 and pp62, confines the core shell and the DNA-containing nucleoid. This architecture represents, to our knowledge, a unique structural organization among known NCLDVs.

Results

ASFV structure

Purified extracellular ASVF virions were analyzed using cryo-EM. Recorded images show a very large icosahedral virus with two differently located membranes (Fig. 1A). The outer envelope, acquired by budding during virus egress, does not follow an icosahedral symmetry. The resolution for the ASFV outer capsid, located beneath the outer envelope, is 23 Å, as judged by the Fourier shell correlation (FSC) at the 0.143 criterion (and $\sim$32 Å at 0.5 FSC; see Fig. 1B, "Experimental procedures", and Table 1). It measures about $\sim$2,050 Å facet-to-facet (outer capsid) and $\sim$2,400 Å vertex-to-vertex (and radially averaged $\sim$2,080 Å in diameter; Fig. 1C), and it is similar in size to only two other NCLDVs, Faustovirus and Medusavirus, determined by cryo-EM at 15 and 31 Å resolution, respectively (28, 29). The outer capsid surrounds an icosahedral membrane whose outer and inner bilayer leaflets are discernible, indicating a resolution for this less-ordered region in the range of 35 Å (Fig. 1C) (35). In turn, the inner membrane contains an icosahedral inner capsid that encloses the core shell and the nucleoid (Fig. 1, C and D).

The cryo-EM map of the outer capsid clearly shows the organization of the pseudo-hexagonal capsomers (Fig. 2, A and B). These are composed of homotrimers of MCP p72 [determined in this study at 4.6 Å resolution as possessing a double jelly-roll fold (see Fig. 2 (C and D), Fig. 3, "Experimental procedures", and Table 1) and very recently by others at 2.67 Å (36)] arranging on a hexagonal lattice with $h = 7$ and $k = 12$, giving a triangulation number of $T = 277$ (Fig. 1B), the same as that found in Faustovirus and Medusavirus. The p72 shell, with a thickness of $\sim$90 Å (Fig. 1C), can thus be described in geometrical terms, as done for other NCLDVs, by trisymmetrons and pentasymmetrons, which are well-ordered collections of capsomers forming the virion facets and vertex regions, respectively (Fig. 2B) (37). The ASFV trisymmetron is made of 120 pseudo-hexagonal capsomers (360 copies of MCP p72), whereas the pentasymmetron contains 30 pseudo-hexagonal capsomers (90 copies of MCP p72) plus 1 penton complex with plausibly five copies of the minor penton protein p49 (B438L) (Fig. 2, A and B), as deduced from the ultrastructural phenotype of a recombinant inducible virus expressing p49 and immunogold labeling (14, 21). The icosahedral asymmetric unit (IAU) is therefore composed of 138 copies of p72 plus 1 copy of the penton protein (as p72 displays two jelly-rolls, $138 \times 2 = 276$ plus 1 copy of penton protein give 277, which recapitulates the T number) (Fig. 2C). This organization replicates the use of the pseudo-hexameric capsomer footprint in capsid assembly also seen in smaller virus members of the PRD1-adenovirus lineage (Fig. 3A) (31, 32). However, this is one of the solutions for viral capsid assembly, as other smaller dsDNA viruses use, for example, coat proteins with the so-called HK97 fold characterized basically by two domains: the P-domain, with a long α-helix and a three-stranded β-sheet, and the A-domain, with two α-helices and a β-sheet (31).

Juxtaposed to the p72 proteinaceous shell, the icosahedrally ordered membrane is apparent, with an overall thickness of $\sim$34 Å (peak-to-peak distance in Fig. 1C) that is in line with
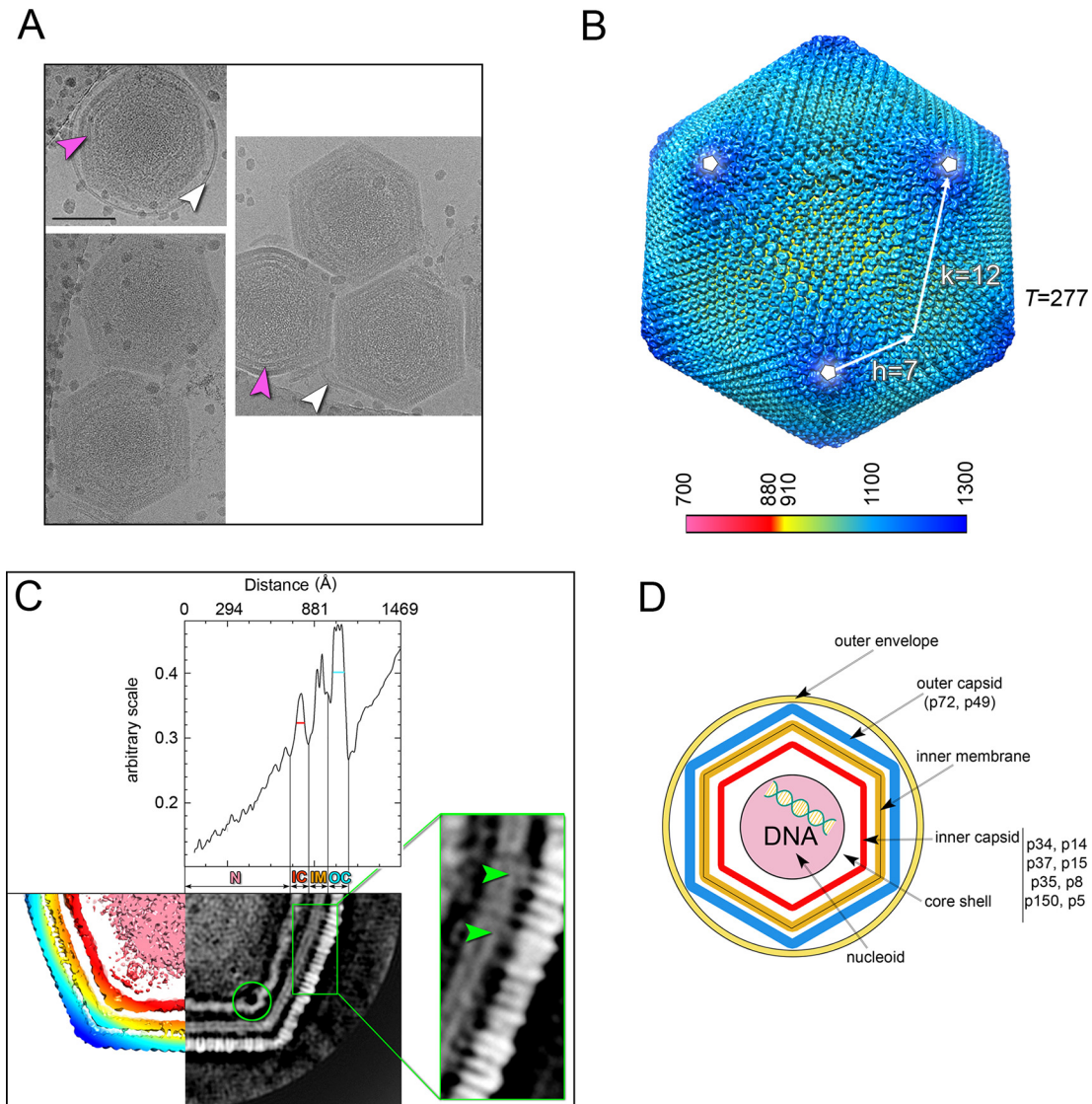
Figure 1. ASFV overall structure. *A*, cryo-images of ASFV virions with some Percoll particles derived from the purification process (see "Experimental procedures"); *white arrowheads* mark the outer envelope of the virion (in some cases broken); *magenta arrowheads* mark the inner membrane. *Scale bar*, 1,000 Å. *B*, *surface rendering* of the ASFV density displayed using Chimera (61) and colored by radial distance (radial *color scale bar* in Å) with the *white arrows* marking the h and k vectors of the hexagonal lattice with triangulation number $T = 277$; the *white pentagons* mark the icosahedral 5-fold axes of a triangular facet. *C*, *left bottom half*, surface-rendered slice of virion density color-coded as Fig. 1*B* with outer capsid and inner membrane at threshold 0.018 (inner capsid and core shell at lower threshold for clarity). *Bottom right*, central section of the 3D reconstructed map of ASFV showing the architectural organization of the different structural components of the virion; the *green rectangle* indicates the region where weak density contacts both capsid and inner membrane, with *green arrowheads* in the *enlarged inset* marking these densities; a *green circle* marks the turreted density at the vertices of the inner capsid. *Top*, radial density profile of the virion density (from the center of the virus to the edge of the box) with *light blue* OC outer capsid, *dark yellow* IM inner membrane, *red* IC inner capsid, and *pink* N nucleoid (*horizontal red* and *cyan lines* show the width used to estimate thickness of both capsids). *D*, *schematic layout* of the ASFV organization as derived from this study with location of some of the viral proteins as from Ref. 14.

other membrane-containing viruses (32, 38, 39). Weak densities across the p72 shell and the outer leaflet of the membrane support the contact of these two architectural constituents (Fig. 1C, inset). At about ~110 Å (peak-to-peak distance) inside from the inner leaflet of the membrane, a further icosahedral structure, the inner capsid, contains the entire core (Fig. 1, C and D). The cryo-EM map shows that this capsid, with a thickness of ~50 Å and with a radial diameter of ~1,580 Å, is composed of capsomers displaying a pseudo-hexameric morphology sitting on an hexagonal array with the triangulation number $T = 19$ (Fig. 4). The center-to-center distance between the capsomers is ~75 Å although further density seems to

occupy the interspace between capsomers, possibly cementing them together (Fig. 4, insets). This value matches the conserved center-to-center distance observed in virus capsid based on vertical double jelly-roll MCPs like those of the PRD1-adenovirus lineage (Fig. 4). At the apices, the density becomes turreted, indicating the presence of a specific penton protein. The protein components of the inner capsid shell are mature products derived from viral polyproteins pp62 (p35, p15, and p8) and pp220 (p5, p14, p34, p37, and p150) (14, 40, 41). When the sequences of the medium size proteins (molecular mass >17 kDa and <42 kDa) were submitted to the Phyre2 protein fold recognition server for sec-
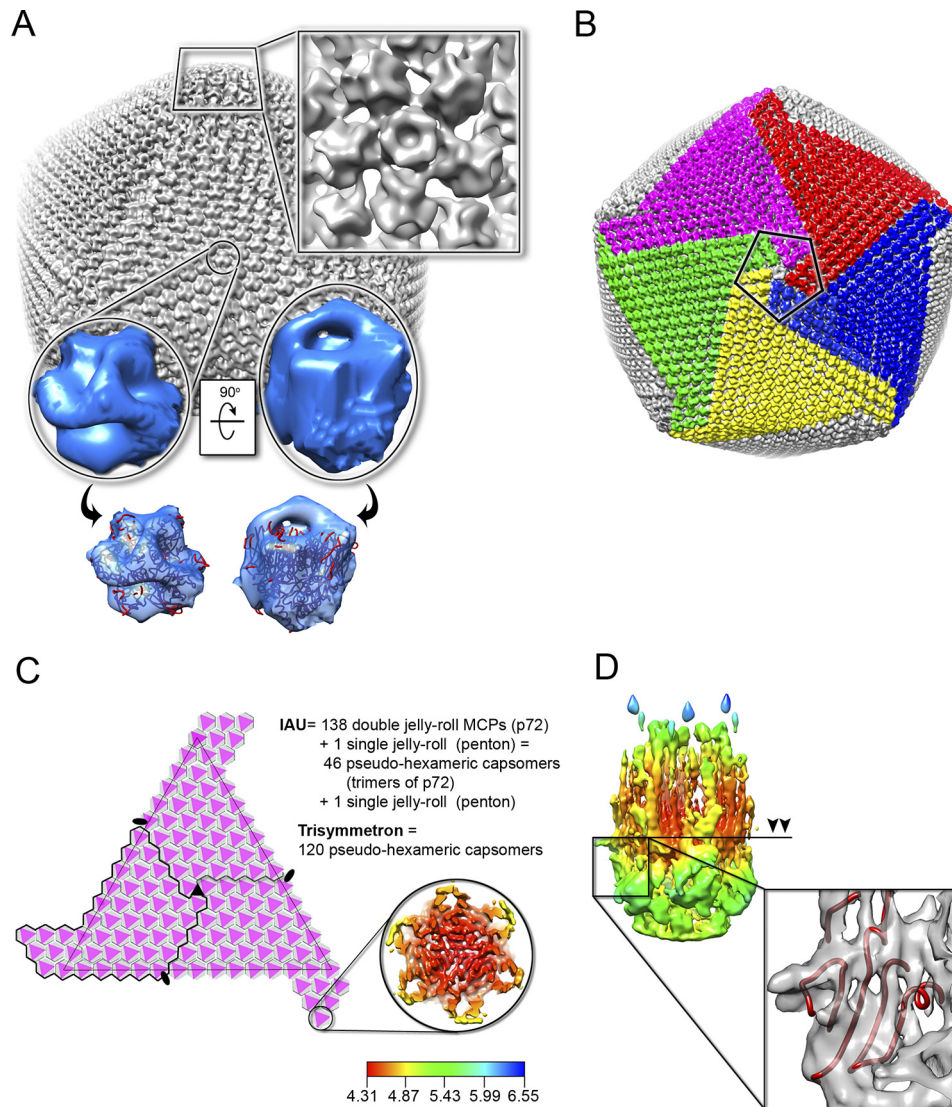
Figure 2. ASFV outer capsid organization and composition. *A,* surface rendering of an ASFV virion facet (*gray*) at 0.024 threshold in Chimera with the *top right inset* showing the penton protein (five copies of putative p49) at the center and peripentonal capsomers (homotrimers of MCP p72) viewed along the icosahedral 5-fold axis. The *insets below* show in *blue* the density corresponding to a capsomer viewed from the top along its 3-fold axis (*left*) and viewed from the side orthogonal to its 3-fold axis (*right*). The *black arrows* point at the same density (40% transparency) in which the atomic model corresponding to a capsomer of Faustovirus composed of three copies of the double jelly-roll MCP (represented as a *cartoon tube* in *red*; PDB entry 5J7O) has been docked (for clarity, only the double jelly-roll core domains have been depicted). *B,* schematic representation of the organization of the trisymmetrons and pentasymmetrons in ASFV; five trisymmetrons are *colored* in *red*, *blue*, *yellow*, *green*, and *magenta*; the pentasymmetron is *outlined* by a *black pentagon* with at its center the penton (*gray density*). *C,* layout of one virion facet (the *black-outlined triangle* marks those capsomers composing a trisymmetron) with *gray hexagons* describing the pseudo-hexameric morphology displayed by MCP p72 trimers depicted as *magenta triangles*. *Black ovals* and a *triangle* mark the 2- and 3-fold icosahedral symmetry axes, respectively, and the *black zig-zag line* defines the capsomers composing the IAU. The *black semi-transparent zig-zag line* stemming from the icosahedral 3-fold identifies the remaining two IAUs of the facet. The *inset* at the *bottom right* is a slice of the cryo-EM map of homotrimers of MCP p72 viewed along the molecular 3-fold axis, and it shows the pseudo-hexameric footprint generated by the p72 protein adopting the double jelly-roll fold (Fig. 3*A*); this is displayed using the local resolution calculated in RELION (60) and mapped (*color-coded* resolution bar in Å) onto the capsomer density at a 0.03 threshold level in Chimera [for details on map interpretability, see "Experimental procedures" and Figs. 3 (*B* and *C*) and 6 (*A* and *B*)]. *D,* rendering of the homotrimeric p72 capsomer as in *C* (*inset*) but viewed perpendicularly to the 3-fold axis (the *horizontal black line* and *arrowheads* show the height at which the density has been sliced in *C* (*inset*), whereas the *black rectangle* marks the region of the *inset* corresponding to a wall of a β-barrel (*gray density* at 0.032 threshold) where the separation of the β-strands is incipient; this density has been fitted with a jelly-roll of Faustovirus MCP (*red cartoon tube*).

ondary structure prediction, p35, p14, p34, and p37 were predicted to be mainly α-helical (>60%) whereas p15 was predicted to be a mixture of α-helices (36%) and β-strands (26%) (42). The determination of whether p15 is the MCP forming the capsomers of this inner capsid, due to its β-strand content, will require a higher-resolution map. The corresponding IAU thus contains three pseudo-hexameric capsomers and one protein at the vertex (Fig. 4). Further

density within the inner capsid corresponds to the presence of the core shell and the nucleoid (Fig. 1, *C* and *D*).
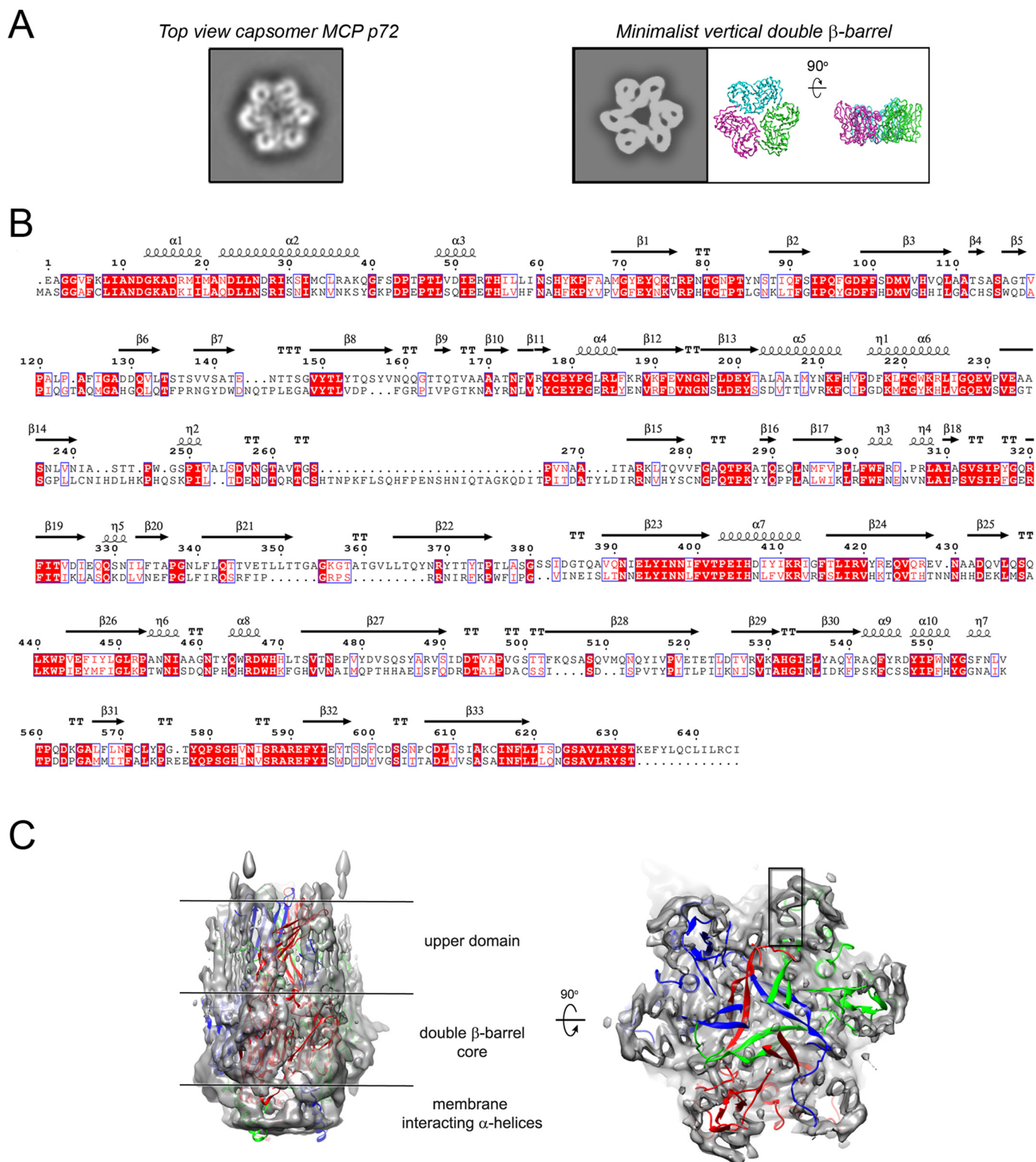
Discussion

Overall architecture of ASFV

Most of NCLDVs possess an icosahedral protein capsid, which is based on a MCP with a double jelly-roll fold, and an

underlying lipoprotein membrane that encloses the genome-containing core (25, 27, 38, 43). An exception to this overall structure is represented by Faustovirus, the closest relative of ASFV (7). The Faustovirus particle, with a diameter of 2,600 Å, lacks an internal membrane but possesses a double-layered protein capsid enclosing the viral genome (28). Its outer layer is composed of a double jelly-roll MCP that is 40% identical to the

ASFV MCP p72 (Fig. 3*B*). The contiguous inner protein layer is assembled by one or more proteins with a likely distinct fold from the jelly-roll (28).

The structure of ASFV appears to combine both architectural components of Faustovirus and those of membrane-containing viruses such as PBCV-1, PRD1, STIV, and Pacmanvirus (11, 32, 38, 44). ASFV possesses two icosahedral concentric cap-
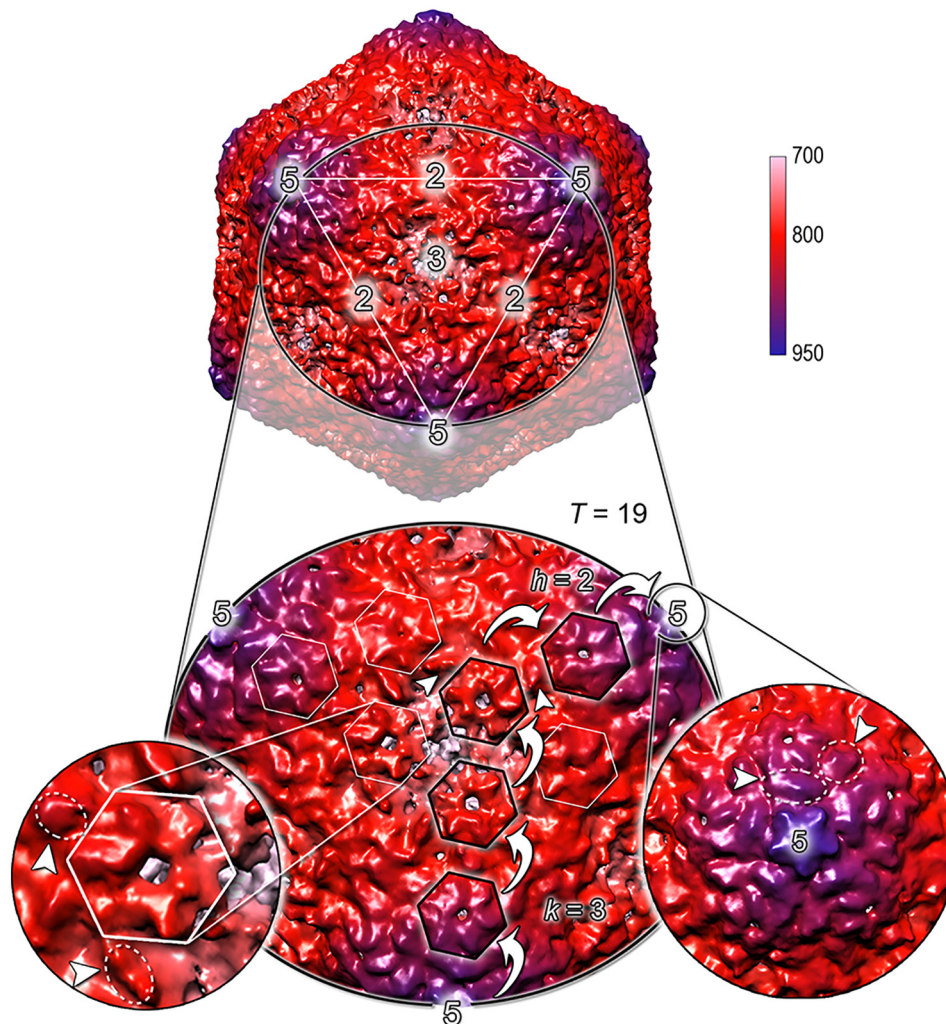

A

Top view capsomer MCP p72

Minimalist vertical double β-barrel

B

C

upper domain

double β-barrel core

membrane interacting α-helices

Figure 4. ASFV inner capsid organization. *Surface representation* of the icosahedral inner capsid *colored* by radial distance (radial *color scale bar* in Å) with the 5-, 3-, and 2-fold icosahedral symmetry axes *labeled* with *cardinal numbers*, and with a *white triangle* marking a facet (the volume was resymmetrized in XMIPP (62), Gaussian filtered with a width of 2.94 Å, and displayed in Chimera at 0.083 threshold). *Inset* below, *enlarged view* of a facet with pseudo-hexameric capsomers marked by *black hexagons* and with *curved white arrows* marking the *h* and *k* vectors of the hexagonal lattice with triangulation number $T = 19$; *white hexagons* mark other capsomers within the facet. *Left insets*, *enlarged views* of (i) a capsomer with the appearance of six petals of a daisy and of (ii) the penton and peripentonal capsomers viewed along the 5-fold axis; additional density in between capsomers is marked by *white arrowheads* and *dotted lines*.

sids interspaced by an icosahedral membrane along with an additional pleomorphic envelope over the outer capsid (Fig. 1, *C* and *D*).

Structure and assembly of the outer capsid

The outer capsid, built from 8,280 MCP p72 copies, is organized in 20 trisymmetrons and 12 pentasymmetrons, composed of 120 and 30 homotrimeric p72 capsomers, respectively.

Further, five copies of the penton protein, putatively the minor capsid protein p49, plug each of the 12 icosahedral vertices. The use of ordered arrays (trisymmetrons and pentasymmetrons) of pseudo-hexameric capsomers allows for large icosahedral capsid to be formed on a curved two-dimensional lattice (26, 37). These large viruses use the pseudo-hexameric capsomers generated by trimers of vertical double jelly-roll MCPs as building blocks, containing a rotational symmetry that facilitates equiv-

Figure 3. Cryo-EM map of homotrimers of MCP p72 purified from the virion at 4.6 Å resolution. *A*, *left*, *top view* of a 2D class-average obtained during 2D classification of ASFV capsomers (composed of MCP p72) unequivocally showing the presence of a pseudo-hexameric symmetry with a true 3-fold axis perpendicular to the viewing plane (no symmetry can be imposed during 2D classification in RELION). *Right*, similar *top view* as on the *left* but density generated by using the known minimalist vertical double β-barrel PDB model with PDB entry 2VVF (represented with a *cartoon tube* and *color-coded* according to chain identity) and corresponding to the MCP P2 of lipid-containing marine bacteriophage PM2 (63). The similarity between the "lobes" corresponding to the individual β-barrels of the two molecules is striking as seen from the *top views*. *B*, the alignment was performed using ClustalW (64) (top Faustovirus sequence and bottom ASFV sequence), and the figure was prepared with ESPript (3) (similarity *color scheme* based on percentage of equivalent residues; *red box*, strict identity; *red character* with *blue frame*, similarity). The secondary structural elements derived from the Faustovirus PDB model (PDB entry 5J7O) are shown as *helices* (α-helix) and *black arrows* (β-strands) at the *top* of the alignment. *C*, fitting in Chimera of the whole trimeric Faustovirus capsomer PDB model (each molecule *differently colored*) into the p72 homotrimeric map (*gray semitransparent*; threshold 0.032). Whereas the overall match in the region corresponding to the double β-barrel core is acceptable, the upper density deviates from the atomic model (see "Experimental procedures"); the *black rectangle* marks the density corresponding to one of the β-barrel walls. The map also shows some density at the base and top that might not belong to the p72, as a consequence of its purification from the virion. The *left* and the *right* densities are not to scale.

alent interactions to be formed. The orientation of these capsomers is equivalent in each trisymmetron, but their orientation across adjacent trisymmetrons is related by a 60° rotation (27). Viruses of the PRD1-adenovirus lineage characterized by possessing a double jelly-roll MCP and smaller in size, use the same pseudo-hexameric capsomer morphology to build the whole triangular facet of the icosahedral particle, leaving space at the vertices only for the five copies of the penton protein, usually with a jelly-roll fold (31, 32, 39). Also, vertical single β-barrel viruses have been found to generate a heterodimeric vertical double jelly-roll with a pseudo-hexagonal shape that recapitulates the close packing seen in vertical double jelly-roll viruses (39). Thus, the use of vertical jelly-roll structures forming capsomers with a pseudo-hexameric footprint offers a means to scale up the size of capsid, exploiting the internal symmetry of these basic building blocks.

The presence of α-helices at the N terminus of ASFV p72 located at the base of the homotrimer (Fig. 3C) (36), and the high hydrophobicity score of the first 10 residues [relative to the first 40 assessed using ProtScale (45)] support a model in which these helices contact the underneath membrane as also seen for PRD1 MCP P3 (32). Further contacts might also occur at the 5-fold vertices between penton proteins and the apex of the inner membrane as observed in membrane-containing viruses, such as STIV and HCIV-1, which interact with the above penton (39, 44). It has been proposed that the capsid assembly of CroV and related giant viruses may initiate at a 5-fold vertex to continuously proceed outward in a spiraling fashion (27), and the same pathway might be used by ASFV.

This progressive spiral assembly might serve, in turn, to organize the icosahedral structures of the underlying membrane and the inner capsid. It is not known, however, which ASFV inner membrane protein(s) may be involved in the interaction with the 5-fold capsid vertex. At present, seven known transmembrane viral proteins [p17 (pD117L), pE183L, p12 (pO61R), p22 (pKP177L), pH108R, pE199L, and pE248R] have been identified on the inner membrane, whereas only one viral protein (pEP402R), a homologue of the T-lymphocyte surface antigen CD2, has been located on the external envelope so far (14). However, about half of the 15 putative transmembrane virion proteins remain uncharacterized (14).

Core organization

In contrast to other known lipid-containing viruses, the inner icosahedral membrane surrounds an icosahedral capsid that encloses the core shell and the central DNA-containing nucleoid (16, 22). This inner capsid, assembled by pseudo-hexameric capsomers, displays a different triangulation number ($T = 19$) than the outer capsid ($T = 277$). The density at the apices, which present a turreted morphology (Fig. 1C) distinct to that of the regions close to the 2- and 3-fold axis (Fig. 4), might indicate specific interaction sites with the above membrane. Such interaction would be consistent with the hierarchical and tightly coordinated assembly of ASFV (16). It has been reported that the correct assembly of the inner capsid and core shell depends on the assembly of the outer capsid and the inner membrane, but not vice versa. Thus, inducible ASFV recombi-

nants in which the expression of the core shell polyproteins pp220 and pp62 is inhibited produce icosahedral core-less particles containing a normal outer capsid over the inner membrane (23, 46). At variance, recombinant viruses in which the expression of MCP p72 is inhibited produce aberrant capsid-less structures formed by unprocessed ASFV polyproteins (20). This structural dependence would explain the fact that both capsids are overall aligned along their relative icosahedral axis despite the lack of direct interactions. Higher-resolution reconstruction will better underpin the spatial relationship between the two capsids.

It is known that after ASFV endocytosis, the incoming particles undergo an acidic pH-driven disassembly in late endosomes that involves the loss of the outer membrane and the outer capsid and the subsequent fusion of the inner membrane (47). As a result, the viral cores are delivered into the cytosol to initiate the transcription of the early viral genes. It is tempting to speculate that the structured inner protein capsid may serve to confine and protect the viral genome from host nucleases as well as from host dsDNA sensors that may activate the innate immune response during the first infection stages (48).

On the other hand, it is interesting to note that Faustovirus and Pacmanvirus encode not yet characterized homologs of the ASFV core shell polyproteins pp220 and pp62 as well as the viral protease (7, 11). This suggests that both viruses may use a solution similar to that used by ASFV for their core organization and genome packaging.

Apart from the structural and sequence homologies with dsDNA Faustovirus, double protein–layered viruses with different capsid arrangements (and *T* numbers) have been found primarily in RNA viruses of the *Reoviridae* family, such as BTV and Reovirus, and in bacteriophage Φ6, where the outer-protein shell serves to introduce the inner shell into the cytoplasm (49–51). The multilayered architecture of the virion, with an outer envelope and an inner membrane between two icosahedral capsids, makes the ASFV structure unique among the NCLDVs.

Conclusions and prospects

Overall, the structure described herein reflects the complexity of ASFV assembly and disassembly and showcases the challenges associated with the identification of strategies to both prevent and control ongoing infections. For instance, the nonessential role of the outer envelope in the ASFV infectivity (24) suggests that the outer capsid may play relevant roles during the virus entry. Consistent with this, neutralizing antibodies to MCP p72 have been reported to inhibit *in vitro* the virus attachment to the host cell (52). The identification of neutralization epitopes as well as of putative binding sites to cell receptors in the capsid proteins can benefit from this and future structural studies on ASFV.

Experimental procedures

Cells, viruses, and antibodies

Vero cells (*Chlorocebus sabaeus* kidney fibroblasts; ATCC number CCL-81) were grown in Dulbecco's modified Eagle's medium containing 10% fetal bovine serum, which was reduced to 2% during viral infection. The Vero cell–adapted ASFV
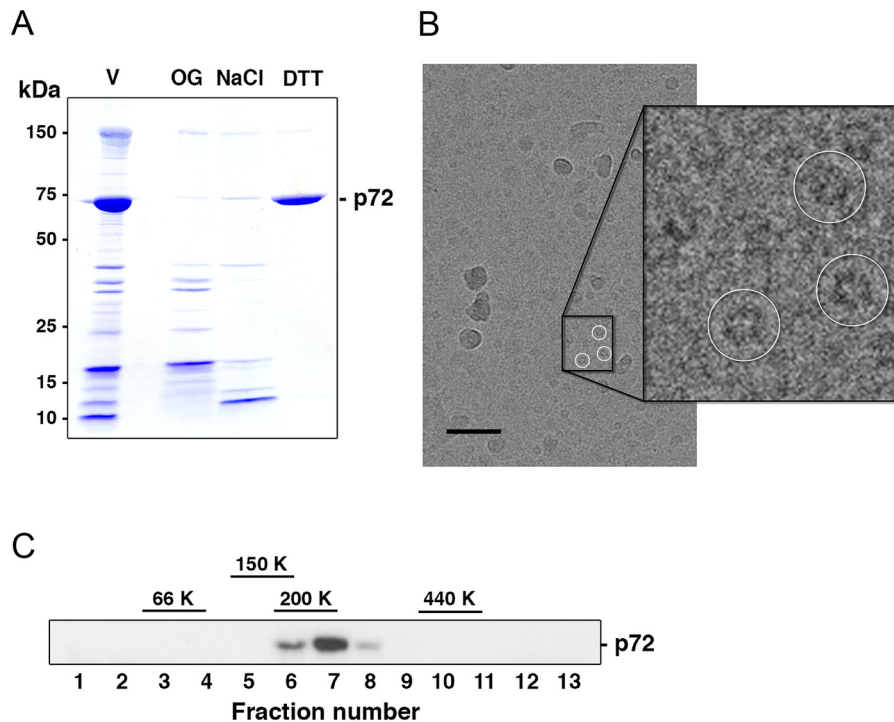
Figure 5. Purification of homotrimers of MCP p72. *A*, MCP p72 was obtained from Percoll-purified virions and analyzed by SDS-PAGE followed by Coomassie Blue staining. ASFV particles were dissociated successively with 1% OG, 0.5 M NaCl, and 0.1 M DTT. The proteins solubilized in each dissociation step were analyzed by SDS-PAGE together with total virus (*V*). *B*, cryo-EM image of virion derived MCP p72 with some Percoll particles present in the sample; *white circles* mark some the capsomers formed by MCP p72 present in the image and extracted for image processing. *Bar*, 50 nm. *C*, sucrose gradient sedimentation of MCP p72. Purified p72 was analyzed through a 10–40% sucrose density gradient in the presence of the indicated molecular weight markers. Gradient fractions were analyzed by Western immunoblotting with an anti-p72 antibody. Note that the p72 sedimentation peak is around the 200-kDa marker.

strain BA71V has already been described (53). The mouse monoclonal antibody 17LD3 against the major capsid protein p72 has also been described previously (19).

ASFV purification

Extracellular ASFV particles were purified according to the Percoll gradient sedimentation method from supernatants of infected Vero cells (54). In brief, extracellular virions were collected at 72 h postinfection from clarified infection supernatants and concentrated by high-speed centrifugation. Then the virus sample was subjected to two successive Percoll (GE Healthcare) density gradient centrifugations, and the obtained virus preparation was further purified by Sephacryl S-1000 (GE Healthcare) gel filtration chromatography. The resulting virus-enriched fractions were collected and concentrated by centrifugation. Purified virus particles were resuspended in PBS and kept at 4 °C until vitrification (Fig. 1*A*).

Purification of MCP p72 from virion

To purify ASFV MCP p72, Percoll-purified extracellular virions were sequentially dissociated as follows. Typically, 200–300 μg of purified viruses were first dissociated with 1% octyl β-D-glucopyranoside (OG) in 10 mM Tris, pH 8.0, for 30 min at 4 °C and then centrifuged at $100,000 \times g$ for 15 min in an A-100/30 Airfuge rotor (Beckman). The sediment was then dissociated for 30 min at 4 °C in 10 mM Tris, pH 8.0, 1% OG, and 500 mM NaCl. Subsequently, the sample was ultracentrifuged as above, and the resulting sediment was incubated for 30 min at 4 °C in 1% OG, 0.5 M NaCl, and 0.1 M DTT in Tris 10 mM pH 8.0.

Finally, the dissociated particles were ultracentrifuged once more at $100,000 \times g$ for 15 min, and the resulting supernatant, containing purified major capsid protein p72, was analyzed either by negative-stain EM, SDS-PAGE and Coomassie staining, or density gradient sedimentation (Fig. 5).

Sample preparation and cryo-EM data collection of MCP p72 and whole virion

MCP p72 sample (4 μl at 0.9–1.2 mg/ml) was pipetted onto 200-mesh Quantifoil R 2/2 graphene oxide–coated grids (to improve particle spread on grid), which were then vitrified using a Vitrobot (Mark III; FEI). Prior to shipping the grids for HR imaging to large EM facilities in northern Europe, such as NeCEN (Netherlands) and Electron Bio-Imaging Centre (eBIC; Diamond Light Source, Harwell, UK) (our gateway to access high-end Titan Krios microscopes) (55), a few of them were checked on the in-house JEM-2200FS/CR (JEOL, Ltd.) electron microscope operating at 200 kV and equipped with a 4K × 4K CCD camera. Forty-frame movies (1,541 total movies) were recorded with a Titan Krios equipped with a Cs corrector and a Falcon-3EC direct detector camera (Thermo Fisher Scientific) with a defocus range from −0.5 to −2.5 μm and total dose of 46.6 $e^-/Å^2$, giving a pixel size of 1.13 Å.

For the preparation of the virion grids, purified ASFV sample at 1.0–1.2 mg/ml was pipetted onto 200-mesh Quantifoil R 2/2 grids, which were vitrified using a Vitrobot (Mark III). Because of the particle's large size, different blot pad positions and blotting times were tested with offset number −2 and 3 s blotting giving satisfactory results in terms of ice thickness relative to

Table 1
Cryo-EM data collection and 3D image processing of whole virion and virion-purified MCP p72

ASFV virion data collection	First data set	Second data set
Nominal magnification	59,000	130,000
Voltage (kV)	300	300
Camera	Falcon-3EC linear	K2 counting
Electron exposure (e$^-$/Å^2)	47.7	47.5
Defocus range (μm)	−0.8 to 2.2	−0.8 to 2.2
Sampling interval (Å/pixel)	1.13	1.09
Movies	8,519	955
Frames	40	60
Selected particles	583	684
Cryo-EM processing	**3D reconstruction**	
Contributing particles	1,110	
Box size (pixel)	1,000	
Pixel size (Å)	2.938	
Symmetry	I2	
Map resolution (Å)	23.0	
FSC threshold	0.143	
Map sharpening *B*-factor (Å^2)	−1235.8	
EMDB code	EMDB-10346	
ASFV MCP p72 data collection		
Nominal magnification	59,000	
Voltage (kV)	300	
Camera	Falcon-3EC counting	
Electron exposure (e$^-$/Å^2)	46.6	
Defocus range (μm)	−0.5 to 2.5	
Sampling interval (Å/pixel)	1.13	
Movies	1,541	
Frames	40	
Selected particles	2,710,425	
Cryo-EM processing	**3D reconstruction**	
Contributing particles	337,803	
Box size (pixel)	192	
Pixel size (Å)	1.13	
Symmetry	C3	
Map resolution (Å)	4.6	
FSC threshold	0.143	
Map sharpening *B*-factor (Å^2)	−320	
EMDB code	EMD-10325	

the particle's size and rupture. Two data sets were acquired for the virion sample. The first one was collected on a Titan Krios equipped with a Cs corrector and a Falcon 3EC direct electron detector in linear mode using the EPU software (Thermo Fisher Scientific). Movies (40 frames) were recorded with a defocus range from −0.8 to −2.2 μm with a dose of 47.7 e$^-$/Å^2 at a nominal magnification of ×59,000, producing a pixel size at the specimen of 1.13 Å (Table 1). Because of the low chance of getting one or two full particles per view using the above set-up (∼1 whole virion per 14 movies), the second ASFV data set was collected more efficiently on a Titan Krios equipped with a Gatan K2 Summit direct electron detector (energy filter slit width of 20 eV) using SerialEM with virtual maps to target each image to individual virions on the grid (56, 57). Movies (60 frames) were recorded in the same defocus range, at a nominal magnification of ×130,000 and a total dose of 47.5 e$^-$/Å^2, producing a pixel size of 1.09 Å at the specimen (Table 1).

Image processing, 3D reconstruction, and analysis

Beam-induced sample motion on recorded frames was corrected using MotionCor2 (58), and the CTF was estimated with CTFFIND4 (59).

For image processing of MCP p72, particle picking was carried out automatically in RELION with a box of 128 × 128 pixels using the Laplacian-of-Gaussian filter for blob detection (60). This led to 2,710,425 objects extracted. This selection was then 2D classified in 20 classes leading to 2,689,946 particles. A further 2D classification in 30 classes cleaned up the initial set to 2,665,492 particles. 2D class-average images already showed the unequivocal presence of a 3-fold axis and the pseudo-hexameric footprint typical of vertical double jelly-roll MCP (Figs. 2C and 3A). This set of particles was 3D classified in three classes using as a starting reference a map generated from the adenovirus hexon trimer (PDB entry 1P2Z) filtered to 60 Å resolution and imposing C3 symmetry (Faustovirus MCP PDB entry 5J7O was not used to avoid potential bias). This process was then repeated, but using as a reference a derived 3D map from a previous class that clearly showed the pseudo-hexameric footprint and overall 3D shapes typical of β-barrels. Out of the three resulting classes (class 1, 46.9%; class 2, 39.2%; class 3, 13.9%), class 3 with 327,803 particles was selected for refinement on the basis of better map interpretability, angular distribution, and estimated resolution. Selected particles were re-extracted with a box size of 192 × 192 pixels and 3D refined with a threshold-derived mask.

Post-processing with a soft mask led to a map with a nominal resolution of 4.6 Å at the 0.143 criterion (Fig. 6A); however, local resolution estimation shows that the resolution is anisotropic, and it ranges from 4.3 to 6.5 Å according to the region of the capsomer (Fig. 2, C and D). This resolution anisotropy and possibly elongated structure [Figs. 2 (C and D) and 3C] might be consequences not only of the presence of top/bottom preferential views (Fig. 6B) but also of the structural flexibility and possibly heterogeneity of a sample that has been dissociated from the virion. All together, the above factors argue for a conservative interpretation of the 3D cryo-EM map of MCP p72 outside the core of the double jelly-roll domain.

For the virion image processing, the following approach was used. From the first data collection, 583 ASFV particles were visually selected and extracted in RELION (60) and 3D classified into two classes (as a reference, an initial symmetrized model was generated in RELION). The largest class with 450 particles was refined, and a preliminary icosahedral model was produced; this model served as reference for the 3D classification of the second data set (684 starting particles), which led to the largest class with 650 particles. Then both set of particles were interpolated to the same pixel size and merged for 3D reconstruction. The merged 1,110 virions were 3D refined in RELION (with "skip-padding" for GPU memory constraints). A threshold mask derived from the outer capsid shell was then used in the latest cycles of refinement until convergence. The corresponding unfiltered half-maps were high-pass filtered to 2,700 Å and used for postprocessing in RELION using a threshold mask with soft edges for the outer capsid (automatic *B*-factor −1,236 Å^2), which led to the final resolution of the ASFV outer capsid of ∼23 Å as judged by the gold-standard FSC at 0.143 (31.6 Å at 0.5 criterion; see Fig. 6C). The discrimination of the outer and inner membrane leaflets of the inner lipid bilayer (a region known to be less ordered than the proteinaceous capsids) usually occurs when the resolution is equal to or higher
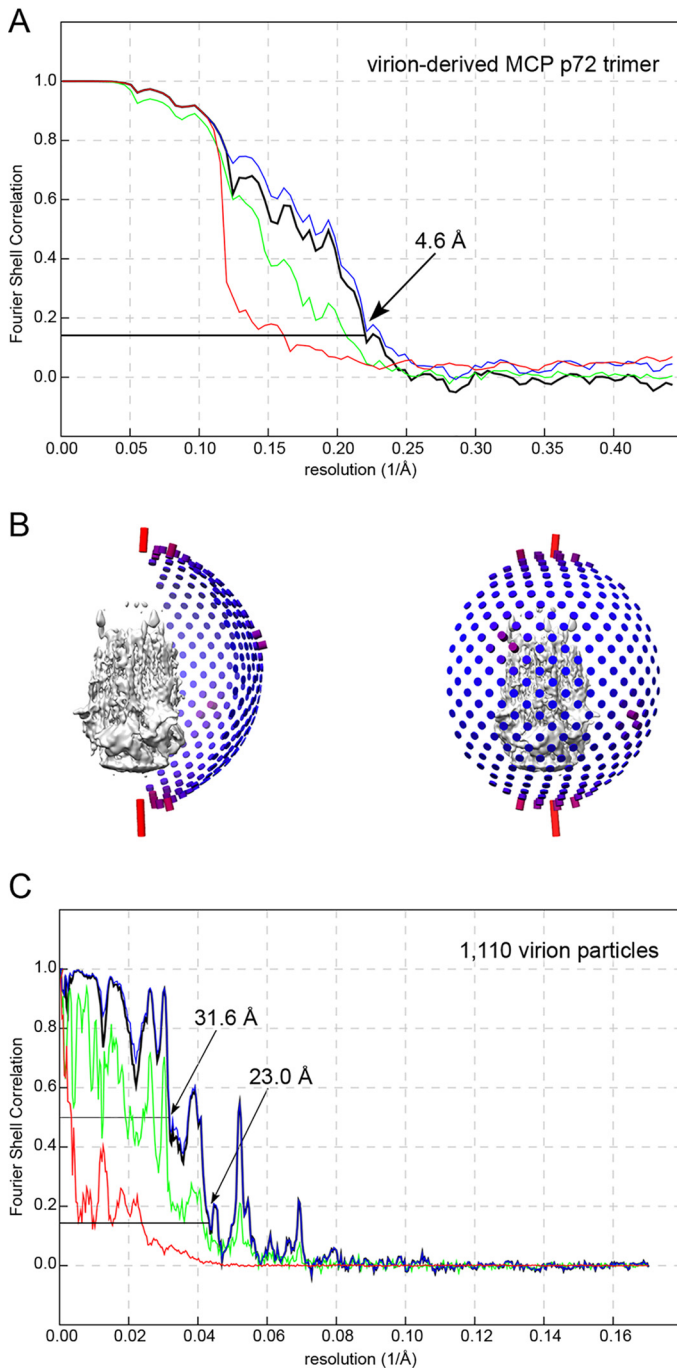
ASBMB

J. Biol. Chem. (2020) 295(1) 1–12 **9**

Figure 6. Fourier shell correlation and Euler angular coverage. *A*, FSC curve of homotrimers of p72 with reported resolution of 4.6 Å at the 0.143 criterion (*black curve*, corrected map; *other colored curves* represent FSC for masked maps (*blue line*), phase-randomized masked maps (*red line*), and unmasked maps (*green line*)) as derived by postprocessing in RELION; for the corresponding local resolution estimation, see Fig. 2 (*C and D*). *B*, different views of the Euler angular coverage of the particles contributing to the 3D reconstruction for the ASFV homotrimeric p72 capsomer from RELION and visualized in Chimera; the *height* of each *cylinder* relates to the number of particles at that Euler angle and shows that the *top* and *bottom views* are overrepresented and caution should be used in interpreting the map outside the double jelly-roll core domain (see Fig. 3C). *C*, FSC curve of ASFV with reported resolution of 23 Å at the 0.143 criterion (*black line*, corrected map; *other colored curves* as in *A*) as derived by postprocessing in RELION. The "spiky" appearance of the FSC curve is due to the limited number of virions (1,110 particles contributing to the final 3D reconstruction) and defocus spread and thus indicates that not all frequencies are equally covered; the map is nevertheless informative. The *horizontal black lines* mark the FSC at 0.5 and 0.143, the latter not hitting the spikes present beyond the 20 Å resolution.

than 35 Å (see the *double peak* in Fig. 1C) (35), thus supporting our resolution estimates. The handedness of the whole ASFV map (*dextro*) was assumed equivalent to that of Faustovirus (28). The resolution for the inner capsid of ∼24.3 Å (FSC at 0.143) was estimated as above using a threshold mask with soft edges delimiting the corresponding protein shell. For visualization, the inner capsid was obtained by subtracting from the refined density of the whole virion the signal corresponding to the outer capsid and inner membrane, and then the box was resized to 600 × 600 × 600 pixels. Map analysis and interpretation was performed in UCFS Chimera (61), which was also used to prepare the figures.

References

1. Dixon, L. K., Sun, H., and Roberts, H. (2019) African swine fever. *Antiviral Res.* **165,** 34–41 CrossRef Medline
2. Revilla, Y., Pérez-Núñez, D., and Richt, J. A. (2018) African swine fever virus biology and vaccine approaches. *Adv. Virus Res.* **100,** 41–74 CrossRef Medline
3. Robert, X., and Gouet, P. (2014) Deciphering key features in protein structures with the new ENDscript server. *Nucleic Acids Res.* **42,** W320–W324 CrossRef Medline
4. Iyer, L. M., Aravind, L., and Koonin, E. V. (2001) Common origin of four diverse families of large eukaryotic DNA viruses. *J. Virol.* **75,** 11720–11734 CrossRef Medline
5. Koonin, E. V., and Yutin, N. (2019) Evolution of the large nucleocytoplasmic DNA viruses of eukaryotes and convergent origins of viral gigantism. *Adv. Virus Res.* **103,** 167–202 CrossRef Medline
6. Philippe, N., Legendre, M., Doutre, G., Couté, Y., Poirot, O., Lescot, M., Arslan, D., Seltzer, V., Bertaux, L., Bruley, C., Garin, J., Claverie, J. M., and Abergel, C. (2013) Pandoraviruses: amoeba viruses with genomes up to 2.5 Mb reaching that of parasitic eukaryotes. *Science* **341,** 281–286 CrossRef Medline
7. Reteno, D. G., Benamar, S., Khalil, J. B., Andreani, J., Armstrong, N., Klose, T., Rossmann, M., Colson, P., Raoult, D., and La Scola, B. (2015) Faustovirus, an asfarvirus-related new lineage of giant viruses infecting amoebae. *J. Virol.* **89,** 6585–6594 CrossRef Medline
8. Legendre, M., Lartigue, A., Bertaux, L., Jeudy, S., Bartoli, J., Lescot, M., Alempic, J. M., Ramus, C., Bruley, C., Labadie, K., Shmakova, L.,

Rivkina, E., Couté, Y., Abergel, C., and Claverie, J. M. (2015) In-depth study of *Mollivirus sibericum*, a new 30,000-y-old giant virus infecting Acanthamoeba. *Proc. Natl. Acad. Sci. U.S.A.* **112,** E5327–E5335 CrossRef Medline

9. Bajrai, L. H., Benamar, S., Azhar, E. I., Robert, C., Levasseur, A., Raoult, D., and La Scola, B. (2016) Kaumoebavirus, a new virus that clusters with faustoviruses and asfarviridae. *Viruses* **8,** E278 CrossRef Medline

10. Andreani, J., Aherfi, S., Bou Khalil, J. Y., Di Pinto, F., Bitam, I., Raoult, D., Colson, P., and La Scola, B. (2016) Cedratvirus, a double-cork structured giant virus, is a distant relative of pithoviruses. *Viruses* **8,** E300 CrossRef Medline

11. Andreani, J., Khalil, J. Y. B., Sevvana, M., Benamar, S., Di Pinto, F., Bitam, I., Colson, P., Klose, T., Rossmann, M. G., Raoult, D., and La Scola, B. (2017) Pacmanvirus, a new giant icosahedral virus at the crossroads between asfarviridae and faustoviruses. *J. Virol.* **91,** e00212-17 CrossRef Medline

12. Yáñez, R. J., Rodríguez, J. M., Nogal, M. L., Yuste, L., Enríquez, C., Rodriguez, J. F., and Viñuela, E. (1995) Analysis of the complete nucleotide sequence of African swine fever virus. *Virology* **208,** 249–278 CrossRef Medline

13. Dixon, L. K., Chapman, D. A., Netherton, C. L., and Upton, C. (2013) African swine fever virus replication and genomics. *Virus Res.* **173,** 3–14 CrossRef Medline

14. Alejo, A., Matamoros, T., Guerra, M., and Andrés, G. (2018) A proteomic atlas of the African swine fever virus particle. *J. Virol.* **92,** e01293-18 CrossRef Medline

15. Carrascosa, J. L., Carazo, J. M., Carrascosa, A. L., García, N., Santisteban, A., and Viñuela, E. (1984) General morphology and capsid fine structure of African swine fever virus particles. *Virology* **132,** 160–172 CrossRef Medline

16. Salas, M. L., and Andrés, G. (2013) African swine fever virus morphogenesis. *Virus Res.* **173,** 29–41 CrossRef Medline

17. Andrés, G., Simón-Mateo, C., and Viñuela, E. (1997) Assembly of African swine fever virus: role of polyprotein pp220. *J. Virol.* **71,** 2331–2341 Medline

18. Andrés, G., García-Escudero, R., Simón-Mateo, C., and Viñuela, E. (1998) African swine fever virus is enveloped by a two-membraned collapsed cisterna derived from the endoplasmic reticulum. *J. Virol.* **72,** 8988–9001 Medline

19. Suarez, C., Andres, G., Kolovou, A., Hoppe, S., Salas, M. L., Walther, P., and Krijnse Locker, J. (2015) African swine fever virus assembles a single membrane derived from rupture of the endoplasmic reticulum. *Cell Microbiol.* **17,** 1683–1698 CrossRef Medline

20. García-Escudero, R., Andrés, G., Almazán, F., and Viñuela, E. (1998) Inducible gene expression from African swine fever virus recombinants: analysis of the major capsid protein p72. *J. Virol.* **72,** 3185–3195 Medline

21. Epifano, C., Krijnse-Locker, J., Salas, M. L., Salas, J., and Rodríguez, J. M. (2006) Generation of filamentous instead of icosahedral particles by repression of African swine fever virus structural protein pB438L. *J. Virol.* **80,** 11456–11466 CrossRef Medline

22. Andrés, G., Alejo, A., Salas, J., and Salas, M. L. (2002) African swine fever virus polyproteins pp220 and pp62 assemble into the core shell. *J. Virol.* **76,** 12473–12482 CrossRef Medline

23. Andrés, G., García-Escudero, R., Salas, M. L., and Rodríguez, J. M. (2002) Repression of African swine fever virus polyprotein pp220-encoding gene leads to the assembly of icosahedral core-less particles. *J. Virol.* **76,** 2654–2666 CrossRef Medline

24. Andrés, G., García-Escudero, R., Viñuela, E., Salas, M. L., and Rodríguez, J. M. (2001) African swine fever virus structural protein pE120R is essential for virus transport from assembly sites to plasma membrane but not for infectivity. *J. Virol.* **75,** 6758–6768 CrossRef Medline

25. Fang, Q., Zhu, D., Agarkova, I., Adhikari, J., Klose, T., Liu, Y., Chen, Z., Sun, Y., Gross, M. L., Van Etten, J. L., Zhang, X., and Rossmann, M. G. (2019) Near-atomic structure of a giant virus. *Nat. Commun.* **10,** 388 CrossRef Medline

26. Yan, X., Yu, Z., Zhang, P., Battisti, A. J., Holdaway, H. A., Chipman, P. R., Bajaj, C., Bergoin, M., Rossmann, M. G., and Baker, T. S. (2009) The capsid proteins of a large, icosahedral dsDNA virus. *J. Mol. Biol.* **385,** 1287–1299 CrossRef Medline

27. Xiao, C., Fischer, M. G., Bolotaulo, D. M., Ulloa-Rondeau, N., Avila, G. A., and Suttle, C. A. (2017) Cryo-EM reconstruction of the *Cafeteria roenbergensis* virus capsid suggests novel assembly pathway for giant viruses. *Sci. Rep.* **7,** 5484 CrossRef Medline

28. Klose, T., Reteno, D. G., Benamar, S., Hollerbach, A., Colson, P., La Scola, B., and Rossmann, M. G. (2016) Structure of faustovirus, a large dsDNA virus. *Proc. Natl. Acad. Sci. U.S.A.* **113,** 6206–6211 CrossRef Medline

29. Yoshikawa, G., Blanc-Mathieu, R., Song, C., Kayama, Y., Mochizuki, T., Murata, K., Ogata, H., and Takemura, M. (2019) Medusavirus, a novel large DNA virus discovered from hot spring water. *J. Virol.* **93,** e02130-18 CrossRef Medline

30. Krupovic, M., and Koonin, E. V. (2017) Multiple origins of viral capsid proteins from cellular ancestors. *Proc. Natl. Acad. Sci. U.S.A.* **114,** E2401–E2410 CrossRef Medline

31. Abrescia, N. G., Bamford, D. H., Grimes, J. M., and Stuart, D. I. (2012) Structure unifies the viral universe. *Annu. Rev. Biochem.* **81,** 795–822 CrossRef Medline

32. Abrescia, N. G., Cockburn, J. J., Grimes, J. M., Sutton, G. C., Diprose, J. M., Butcher, S. J., Fuller, S. D., San Martín, C., Burnett, R. M., Stuart, D. I., Bamford, D. H., and Bamford, J. K. (2004) Insights into assembly from structural analysis of bacteriophage PRD1. *Nature* **432,** 68–74 CrossRef Medline

33. Abergel, C., Legendre, M., and Claverie, J. M. (2015) The rapidly expanding universe of giant viruses: *Mimivirus, Pandoravirus, Pithovirus* and *Mollivirus. FEMS Microbiol Rev.* **39,** 779–796 CrossRef Medline

34. Bahar, M. W., Graham, S. C., Stuart, D. I., and Grimes, J. M. (2011) Insights into the evolution of a complex virus from the crystal structure of vaccinia virus D13. *Structure* **19,** 1011–1020 CrossRef Medline

35. Cockburn, J. J., Abrescia, N. G., Grimes, J. M., Sutton, G. C., Diprose, J. M., Benevides, J. M., Thomas, G. J., Jr., Bamford, J. K., Bamford, D. H., and Stuart, D. I. (2004) Membrane structure and interactions with protein and DNA in bacteriophage PRD1. *Nature* **432,** 122–125 CrossRef Medline

36. Liu, Q., Ma, B., Qian, N., Zhang, F., Tan, X., Lei, J., and Xiang, Y. (2019) Structure of the African swine fever virus major capsid protein p72. *Cell Res.* 10.1038/s41422–019-0232-x CrossRef Medline

37. Sinkovits, R. S., and Baker, T. S. (2010) A tale of two symmetrons: rules for construction of icosahedral capsids from trisymmetrons and pentasymmetrons. *J. Struct. Biol.* **170,** 109–116 CrossRef Medline

38. Yan, X., Olson, N. H., Van Etten, J. L., Bergoin, M., Rossmann, M. G., and Baker, T. S. (2000) Structure and assembly of large lipid-containing dsDNA viruses. *Nat. Struct. Biol.* **7,** 101–103 CrossRef Medline

39. Santos-Pérez, I., Charro, D., Gil-Carton, D., Azkargorta, M., Elortza, F., Bamford, D. H., Oksanen, H. M., and Abrescia, N. G. A. (2019) Structural basis for assembly of vertical single β-barrel viruses. *Nat. Commun.* **10,** 1184 CrossRef Medline

40. Simón-Mateo, C., Andrés, G., and Viñuela, E. (1993) Polyprotein processing in African swine fever virus: a novel gene expression strategy for a DNA virus. *EMBO J.* **12,** 2977–2987 CrossRef Medline

41. Simón-Mateo, C., Andrés, G., Almazán, F., and Viñuela, E. (1997) Proteolytic processing in African swine fever virus: evidence for a new structural polyprotein, pp62. *J. Virol.* **71,** 5799–5804 Medline

42. Kelley, L. A., Mezulis, S., Yates, C. M., Wass, M. N., and Sternberg, M. J. (2015) The Phyre2 web portal for protein modeling, prediction and analysis. *Nat. Protoc.* **10,** 845–858 CrossRef Medline

43. Xiao, C., Kuznetsov, Y. G., Sun, S., Hafenstein, S. L., Kostyuchenko, V. A., Chipman, P. R., Suzan-Monti, M., Raoult, D., McPherson, A., and Rossmann, M. G. (2009) Structural studies of the giant mimivirus. *PLos Biol.* **7,** e92 CrossRef Medline

44. Veesler, D., Ng, T. S., Sendamarai, A. K., Eilers, B. J., Lawrence, C. M., Lok, S. M., Young, M. J., Johnson, J. E., and Fu, C. Y. (2013) Atomic structure of the 75 MDa extremophile *Sulfolobus* turreted icosahedral virus determined by cryoEM and X-ray crystallography. *Proc. Natl. Acad. Sci. U.S.A.* **110,** 5504–5509 CrossRef Medline

45. Gasteiger, E., Hoogland, C., Gattiker, A., Duvaud, S., Wilkins, M. R., Appel, R. D., Bairoch, A. (2005) Protein identification and analysis tools on the

ExPASy server. In *The Proteomics Protocols Handbook* (Walker, J. M., ed) pp. 571–607, Humana Press, Totowa, NJ

46. Suárez, C., Salas, M. L., and Rodríguez, J. M. (2010) African swine fever virus polyprotein pp62 is essential for viral core development. *J. Virol.* **84,** 176–187 CrossRef Medline

47. Hernáez, B., Guerra, M., Salas, M. L., and Andrés, G. (2016) African swine fever virus undergoes outer envelope disruption, capsid disassembly and inner envelope fusion before core release from multivesicular endosomes. *PLoS Pathog.* **12,** e1005595 CrossRef Medline

48. Wu, J., and Chen, Z. J. (2014) Innate immune sensing and signaling of cytosolic nucleic acids. *Annu. Rev. Immunol.* **32,** 461–488 CrossRef Medline

49. Grimes, J., Basak, A. K., Roy, P., and Stuart, D. (1995) The crystal structure of bluetongue virus VP7. *Nature* **373,** 167–170 CrossRef Medline

50. Reinisch, K. M., Nibert, M. L., and Harrison, S. C. (2000) Structure of the reovirus core at 3.6 Å resolution. *Nature* **404,** 960–967 CrossRef Medline

51. Huiskonen, J. T., de Haas, F., Bubeck, D., Bamford, D. H., Fuller, S. D., and Butcher, S. J. (2006) Structure of the bacteriophage ϕ6 nucleocapsid suggests a mechanism for sequential RNA packaging. *Structure* **14,** 1039–1048 CrossRef Medline

52. Gómez-Puertas, P., Rodríguez, F., Oviedo, J. M., Ramiro-Ibáñez, F., Ruiz-Gonzalvo, F., Alonso, C., and Escribano, J. M. (1996) Neutralizing antibodies to different proteins of African swine fever virus inhibit both virus attachment and internalization. *J. Virol.* **70,** 5689–5694 Medline

53. Enjuanes, L., Carrascosa, A. L., Moreno, M. A., and Viñuela, E. (1976) Titration of African swine fever (ASF) virus. *J. Gen. Virol.* **32,** 471–477 CrossRef Medline

54. Carrascosa, A. L., del Val, M., Santarén, J. F., and Viñuela, E. (1985) Purification and properties of African swine fever virus. *J. Virol.* **54,** 337–344 Medline

55. Stuart, D. I., Subramaniam, S., and Abrescia, N. G. (2016) The democratization of cryo-EM. *Nat. Methods* **13,** 607–608 CrossRef Medline

56. Mastronarde, D. N. (2005) Automated electron microscope tomography using robust prediction of specimen movements. *J. Struct. Biol.* **152,** 36–51 CrossRef Medline

57. Schorb, M., Haberbosch, I., Hagen, W. J. H., Schwab, Y., and Mastronarde, D. N. (2019) Software tools for automated transmission electron microscopy. *Nat. Methods* **16,** 471–477 CrossRef Medline

58. Zheng, S. Q., Palovcak, E., Armache, J. P., Verba, K. A., Cheng, Y., and Agard, D. A. (2017) MotionCor2: anisotropic correction of beam-induced motion for improved cryo-electron microscopy. *Nat. Methods* **14,** 331–332 CrossRef Medline

59. Rohou, A., and Grigorieff, N. (2015) CTFFIND4: fast and accurate defocus estimation from electron micrographs. *J. Struct. Biol.* **192,** 216–221 CrossRef Medline

60. Zivanov, J., Nakane, T., Forsberg, B. O., Kimanius, D., Hagen, W. J., Lindahl, E., and Scheres, S. H. (2018) New tools for automated high-resolution cryo-EM structure determination in RELION-3. *Elife* **7,** e42166 CrossRef Medline

61. Pettersen, E. F., Goddard, T. D., Huang, C. C., Couch, G. S., Greenblatt, D. M., Meng, E. C., and Ferrin, T. E. (2004) UCSF Chimera–a visualization system for exploratory research and analysis. *J. Comput. Chem.* **25,** 1605–1612 CrossRef Medline

62. de la Rosa-Trevín, J. M., Otón, J., Marabini, R., Zaldívar, A., Vargas, J., Carazo, J. M., and Sorzano, C. O. (2013) Xmipp 3.0: an improved software suite for image processing in electron microscopy. *J. Struct. Biol.* **184,** 321–328 CrossRef Medline

63. Abrescia, N. G., Grimes, J. M., Kivelä, H. M., Assenberg, R., Sutton, G. C., Butcher, S. J., Bamford, J. K., Bamford, D. H., and Stuart, D. I. (2008) Insights into virus evolution and membrane biogenesis from the structure of the marine lipid-containing bacteriophage PM2. *Mol. Cell* **31,** 749–761 CrossRef Medline

64. Larkin, M. A., Blackshields, G., Brown, N. P., Chenna, R., McGettigan, P. A., McWilliam, H., Valentin, F., Wallace, I. M., Wilm, A., Lopez, R., Thompson, J. D., Gibson, T. J., and Higgins, D. G. (2007) Clustal W and Clustal X version 2.0. *Bioinformatics* **23,** 2947–2948 CrossRef Medline

ASBMB